Smart Charge Management of Photovoltaic using Burp Charge System on Energy-Saving Configuration with Fast Tracking Algorithm

Krishna Mohan Das
Assistant Professor
Einstein Academy of Technology & Management, India

B. Krishnapriya
Assistant Professor
Einstein Academy of Technology & Management, India

Subhasis Tripathy
Assistant Professor
Einstein Academy of Technology & Management, India

Snigdha Sarangi
Assistant Professor
Einstein Academy of Technology & Management, India

Abstract

Recently, renewable energy has been significantly attractive to our life facing on the alternative energy sources possibly to replace the fossil energy. Except for the renewable energy directly converting to grid, green house, and so on, the applications through indirect conversion are still the focus of attention, especially for such as standalone system, mobile solar charger, hybrid system, and so on. However, converters are always indirectly via a battery-regulated dc bus to capture renewable energy, which is fairly common practice. To achieve pulse charge using direct photovoltaic (PV) energy, it is necessary to keep the energy supply from PV module continuous and optimum, especially to prevent energy supply from interrupting during the pulse break period. To perform the mentioned idea, a PV burp charge system (PV-BCS) proposed is to make PV energy pump continuous with optimum maximum power point tracking (MPPT), which increases the PV utilization, and to dispatch the remaining PV energy for further storage in the pulse break period. A smart charging management (CM) presents three kinds of charge statuses, a burp pulse (BP) charge and two pulse charges, which charges three batteries, B_m, B1, and B2 concurrently and individually. The two pulse charges provided are for accompanying the BP charge in order to keep the PV energy supply continuous and cherish the remaining energy for further storage. The BP charge for B_{mis} composed of a positive pulse (PP) charge in a positive burp pulse (PBP) period and negative pulse (NP) charge in non-PBP period. The other two batteries B1 and B2 are always with PP charge in the non-PBP period, in which B1 charges the remaining PV energy to keep the PV energy supply continuous, realizing the energy treasuring concept; B2 charges the discharge amount from B_m by intensely discharging, which indeed is equivalent to the NP charge, achieving the energy recovery concept.

Keywords: Photo voltaic power, battery charging, smart charging, maximum power point tracking, reduced power mode

---

I. INTRODUCTION

PV burp charge system (PV-BCS) proposed is to make PV energy pump continuous with optimum PWM Generation using Control loop operation, which increases the PV utilization and to dispatch the remaining PV energy for further storage in the pulse break period. Some of the fast charging systems presently available incorporate negative pulse fast charging algorithms that claim to have great benefits to batteries including reduced recharge time, lower temperature rise, full recharge capabilities, as well as shorter equalization times. In the present system model draw backs in the existing model was rectified by developing Smart management system with three charge state. Power is made to available throughout the day. Maximum power is obtained from the solar system. Fly back converter is implemented. Life of the battery is improved. Since the older systems were having problems with fail in tracking maximum power from solar system. No effective charge management is implemented. Safety in the converter unit is poor. Shortens the life of battery.

This paper presents a fast maximum power point Tracking (MPPT) control algorithm for the photovoltaic (PV) in which the PV generator may also need to work in a reduced power mode (RPM) to avoid dynamic overloading. The two control modes, MPPT and RPM, are inherently compatible and can be readily implemented, without the need of a dumping load for the RPM. Following the establishment of a dynamic system model, the study develops the guidelines to determine the variables of a direct hill-climbing method for MPPT the perturbation time intervals and the magnitudes of the applied perturbations. These results are then used to optimally set up a variable-step size incremental conductance (VSIC) algorithm along with adaptive RPM control. The power tracking performance and power limiting capability are verified by simulation and experiment.

To date, it seems a general way to execute pulse charging through a battery-regulated dc bus if the energy supply is from PV module. Moreover, most charging processes using PV supply always use constant-current and constant-voltage (CC-CV) strategy. In this paper, a photovoltaic burp charge system (PV-BCS) is proposed to perform the pulse charge with direct PV energy supply without using dc bus through an additional dc/dc converter. In reality, if a pulse charger is to be used in a PV system without using

dc bus as energy buffer, it may happen that the PV energy supply will interrupt during the pulse break period. As a result, the maximum power point tracking (MPPT) may be intermittent to lose the tracking optimization. However, the proposed PV- BCS not only can make MPPT continuous for increasing the PV utilization, but also can dispatch and store the remaining PV energy for energy saving during the pulse break period, achieving energy treasuring and recovery concept. Residential photovoltaic (PV) installations exceeded 21 GW by the end of 2011. It was estimated that the rate of increase in the last year (2012) would be 60%, and over 85% of the added power would come from units below 20 kW. This study is concerned with the control of small-scale PV installations, to provide fast maximum power point tracking (MPPT) during normal operation as well as to limit the power level when it becomes excessive. The main enhancement of the study is a solution regarding the overloading of the system which has happened in many occasions. The problem directed to this research is the high-power, low-frequency oscillations that can happen during wind turbine soft stalling, overloading the system up to 1.5 times of the rated power. The reduced power mode (RPM) of operation as proposed in this study can be used to suppress the oscillation due to the fast response of the PV generator. Furthermore, excessive solar radiation at a low temperature can also overload the power electronics in the system. Therefore, RPM is essential to limit the power extracted from the PV array to avoid damaging the downstream circuit. Power limiting may also be called upon in islanded, small-scale hybrid systems when the energy storage is full.

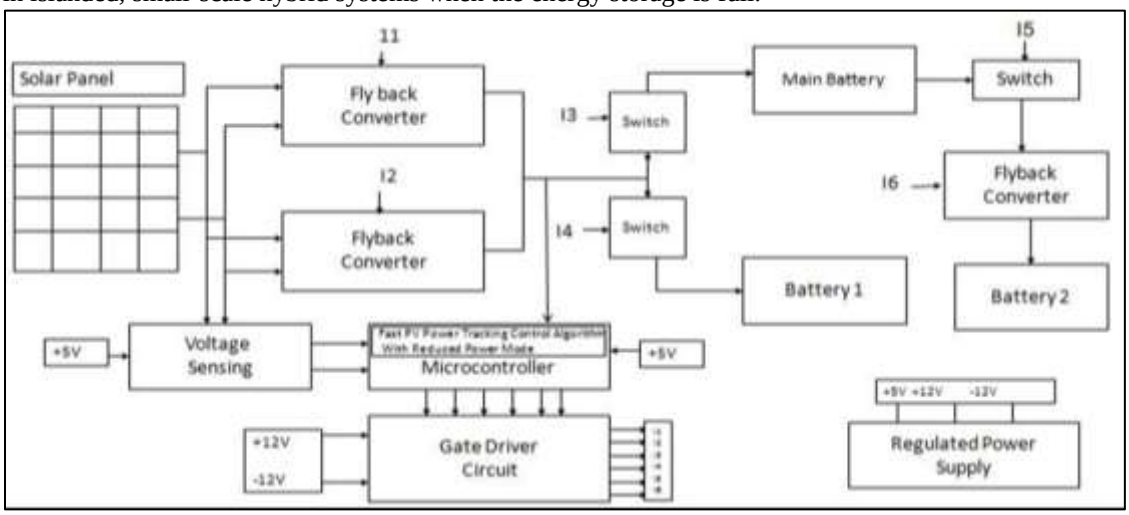

Fig. 1: Block diagram of the burp charger with fast charging method

As displayed in the smart charging management (CM) presented in the PV-BCS is to concurrently charge three batteries, including a burp pulse (BP) charging to a main battery B_m and two PP charging to two accessory batteries B1and B2. The battery B1 is to sustain the continuity of the PV energy supply at optimum MPPT; the battery B2 is to accept the discharging energy from B_m through a fly back converter for example. Although the charging times of the three batteries are not the same, this idea can be tried to apply in a large-scale energy storage site, such as the battery exchange station for electric vehicle When one of the three batteries is fully charged, a new battery can be independently replaced to continue charging while the other two batteries will keep their charging, not being affected by the battery replacement. In other words, the charging of the three batteries is independent in PV-BCS, in which any one of the batteries can be replaced if fully charged. Above all, it is a new try that all the mentioned pulses are formed by high-frequency tiny pulses, which are generated through an interleaved fly back converter (IFC-1) from PV module. The charging waveforms and statuses of the PV-BCS are described in which the BP is simply composed of a PP, a NP, and a pulse break. In order not to interrupt the energy supply from PV module and keep MPPT continuous, a power switch pair QT1 and QT2 complementarily controls the PV energy in PP form to charge the main B_m through QT 1 in the PBP charging period (tp1) forms a BP period Ts2 = tp1+tp2 , achieving the energy treasuring concept. In the non-PBP period, the main B_m will essentially execute NP charge in tp3 and then break for relaxation in tb. However, using an intense discharge to replace the NP charge, the discharge amount from the main B_m can then be transferred to charge the battery B2 through a fly back converter (IFC-2), realizing the energy recovery concept. In this paper, an incremental-conductance (INC) MPPT for example is utilized to guide the IFC-1 that pumps PV energy into a pulse train with a high-frequency to be a charging source. Modeling of IFC-1 to match the characteristic of PV module for maximum power transfer is studied as well. An elaborated experiment was demonstrated to validate the behavior of PV-BCS and compared with a traditional CC-CV charge. Under equivalent charging rate of 0.2 C (where 1 C = 45 AH), when reaching 85% of SOC, the burp charge, compared with the CC-CV charge, is faster than 6.32% of the charging time. Meanwhile, the two batteries B1 and B2 can indeed receive 13 AH, about 30% of SOC, in the non-PBP charging period.

II. PHOTOVOLTAIC BURP CHARGE SYSTEM WITH SMART CHARGE MANAGEMENT

A. Circuit Configuration

The circuit and charging status of the PV-BCS as shown in Fig. 1, can be arranged as shown in Figs. 2(a) and 2(b), including a pair of power switches, an inter-leaved IFC-1 for energy pump from PV module, QT 1 & QT 2 for passing the PV energy

complementarily to charge B_m and B1, a power switch QT 3 for linking an IFC-2 to charge B2 from the discharge of Bm. Two fly-back converters (IFC-1) include with each other to generate high-frequency tiny pulse train as a charging source from the PV module with optimal MPPT.

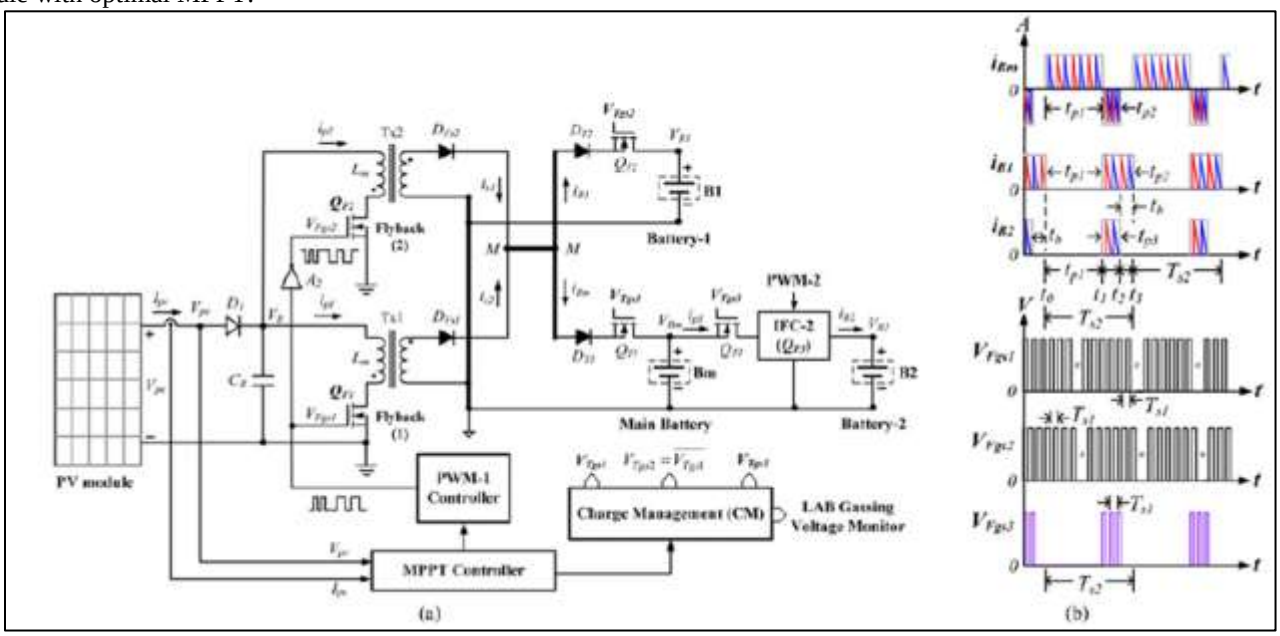

Fig. 2: (a) Realization circuit of the proposed PV-BCS and (b) Charging behaviors of B_m, B1, and B2; gate drives of the interleaved converters IFCs), QF 1, QF 2 , and QF 3 : VF gs1, VF gs2, and VF gs3, respectively; where Ts1 is the high-frequency switching period for IFCs and Ts2 the low-frequency BP period.

All pulses composed of the tiny pulses are achieved by the mentioned three power switches QT1, QT2, and QT3, which take place considering to the BP charging period Ts2. The BP charge for B_m is formed by the actions of QT1 for generating PP in tp1, QT3 for NP in tp3, and a break time tb; the PP charge for B1 via QT2 in tp2, and for B2 via QT3 in tp3 respectively. The complementary action of QT1 and QT2 ensures the PV energy pump is continuous and keeps MPPT at optimum level. Also, it is an easy way to monitor the battery status by using an analog comparison with a gassing reference, which is applicable in real system. In this paper, the detect monitor is embedded in the smart CM, not shown in the circuit of Fig. 2(a), which can instantly detect the battery status with an usual specification around 13.8 V for LAB, where the 13.8 V is corresponding to 100% SOC. In Fig. 2(b), the high-frequency tiny pulse train is synthesized at node M by the two interleaved tiny pulse trains (is1 and is2) that generate at the secondary side of IFC-1. Through QT1, the current train is fragmented into a PP with pulse width the same as the PBP period tp1, and charges the main Bm. Successively, in the non-PBP period, a PP of is with pulse width tp2 through QT2 charges B1. Through QT3, the intense discharge instead of the NP charge is executed by IFC-2, which draws the discharge current from B_{min} (a windowed pulse), composed of high-frequency tiny pulses, with pulse width tp3 that is the NP period. In addition, the gate drives VF gs1 and VF gs2 guided by MPPT for IFC-1 and VF gs3 for IFC-2 are also described in Fig. 2(b). Moreover, the IFC-1 is designed to operate in discontinuous-conduction mode (DCM) with variable-frequency constant-duty (VFCD) control so as to succeed interleave energy pump without pulse aliasing as well as to match the PV module for maximum power transfer.

B. Smart Charging Management

According to the timing diagram shown in Fig. 2(b), three dynamic charging states in one BP charging period Ts2 are successively described in Fig. 3: 1) As shown in Fig. 3(a), Executing the PP Charge to the Main Battery Bm in PBP Period $t0 < t < t1$. The main Bm first receives PP iB1 split from current source is via power switch QT1 in the interval tp1 (PBP period, from t0 to t1) while B1 and B2 are in relaxation state. In this state, the Bm undergoes the PP charging. 2) As in Fig. 3(b), Executing (a) the Intense Discharge from the Bm to B2 and (b) the PP Charge to the B1, $t1<t< t21$) QT1 turns OFF and QT3 turns ON, in the interval tp3 (NP period, from t1 to t2), the IFC-2 intensely discharges the Bm and transfers its discharging amount to charge B2, which performs energy recovery concept. In this situation, the Bm evenly undergoes the NP charging. In this period, which is a part interval of the non-PBP period T2, QT2 turns ON and QT1 turns OFF, B1 first executes part of the residual PP charging from PV module through QT2. This charging action ensures the energy pump from PV module continuously and retains optimum MPPT, attaining energy treasuring concept. 3) As per Fig. 3(c), Continuously Executing the PP Charge to B1, $t2 < t < t3$, ($t3 = T$) and Relaxing Bm, in the interval tb from t2 to t3, which is the part interval of the non-PBP period T2, QT3 turns OFF and QT3 keeps ON, the B1 continues the remaining PP charging from the PV module while the Bm is relaxed until the next new charging cycle. In this situation, Bm and B2 are both in relaxation. For clear description of the charging behaviors, the dynamic status of the charging currents with reference to the three power switches, QT1, QT2, and QT3, are anticipated in Fig. 4, in which some amplitude fluctuations are provided in response to the solar insolation change.

III. MODELING & ANALYSIS OF INTERLEAVED FLYBACK CONVERTERS WITH PV MODULE

A. Modeling of IFC-1 With PV Module Fig. 5(a) shows the simplified circuit of IFC-1, in which the inner resistance γ_{Lm} of the transformer is neglected and all parameters of the two fly-back converters and PV module are assumed to be the same for the simplicity of analysis. The currents ip1,2 drawn from the PV module and the currents is 1, 2 that charge the batteries through the IFC-1 are predicted in Fig. 5(b), in which the peak PV current $i_{p1} = i_{pv1}$ can be given by

$$i_{pv1} = \frac{V_{pv}}{L_m} t_{on} \qquad (1)$$

The average current I_{pv1} in the drawing period T_{s1} is obtained as

$$Ipv_1 = \frac{Vp_v d^2}{2L_m f^{s1}} \qquad (2)$$

where d is duty cycle, Lm magnetizing inductance, and fs1 switching frequency. The PV currents Ipv1 and Ipv2 are presumed to be equal and the average total PV current Ipv from (2) will be

$$I_{pv} = \frac{V_{pv} d^2}{L_m f_{s1}} \qquad (3)$$

If power efficiency η is considered, the output power Po and input power Ppv under the IFC-1 loaded with a battery VB can be given by

$$\eta I_{pv} V_{pv} = I_8 V_B \qquad (4)$$

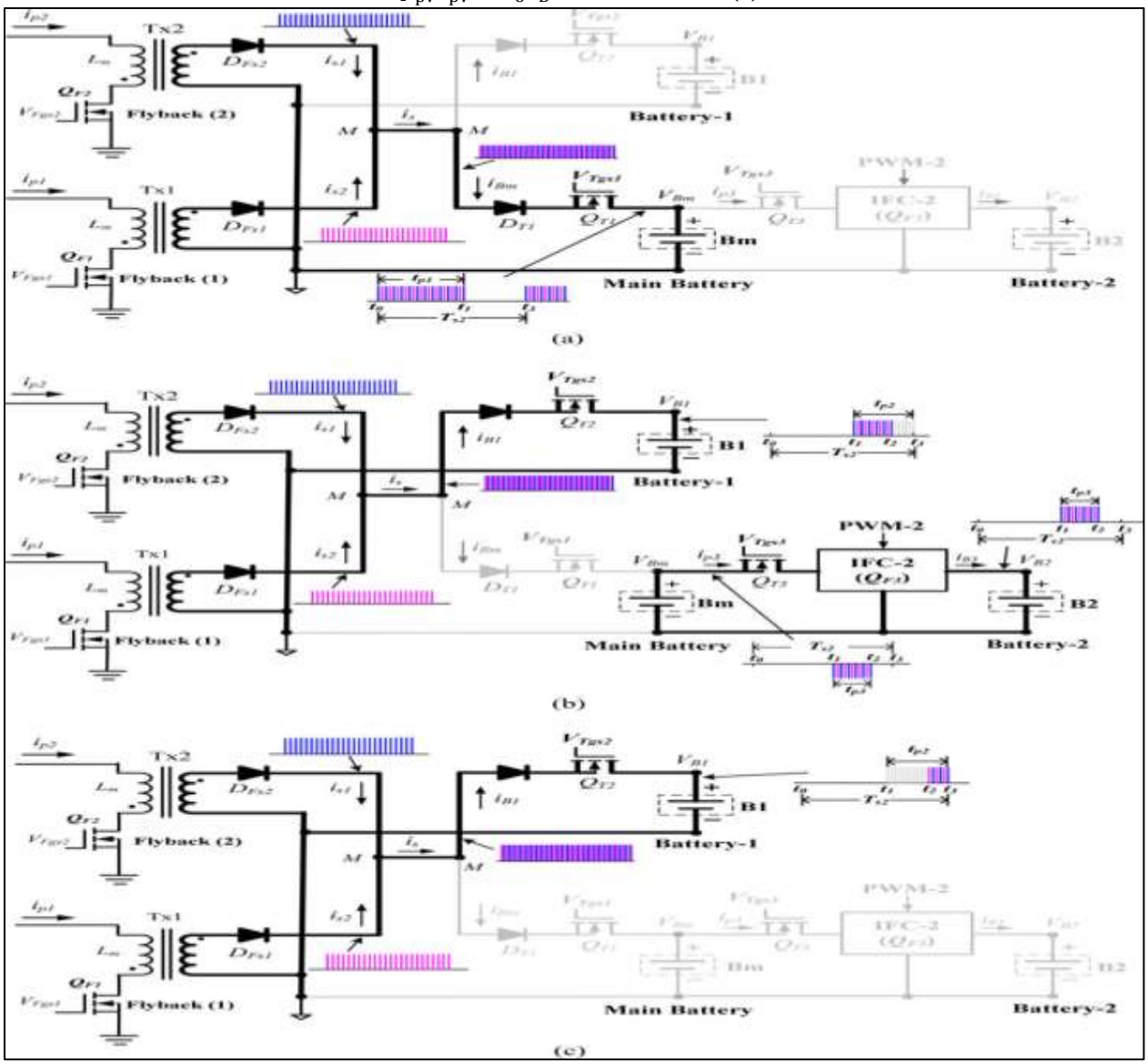

Fig. 3: Dynamic charging behaviors of PV-BCS, (a) Bm executes the PP charging from PV supply during tp 1 while B1 and B2 are relaxed, (b) B1 performs charging with PP from PV supply in part interval of tp 2 and temporarily stops at t2 ; in the meantime, Bm intensely discharges with NP via IFC-2 and in turn to charge B2 with PP, equivalent to NP charging, during tp 3 (where tp 3 < tp 2); and (c) finally, B1 continues charging with the remaining PP from PV supply in the interval of tb, which is part of tp 2; both Bm and B2 are both relaxed until next new charging cycle.

where $V_o = V_B$, $P_o = I_s V_B$, and $P_{pv} = I_{pv} V_{pv}$. The output current I_s and power P_o can then be obtained from (3) and (4) as

$$I_8 = \frac{\eta(V_{pv}d)^2}{V_B L_m f_{s1}} \qquad (5)$$

and the output power

$$P_0 = \frac{\eta(V_{pv}d)^2}{L_m f_{s1}} \qquad (6)$$

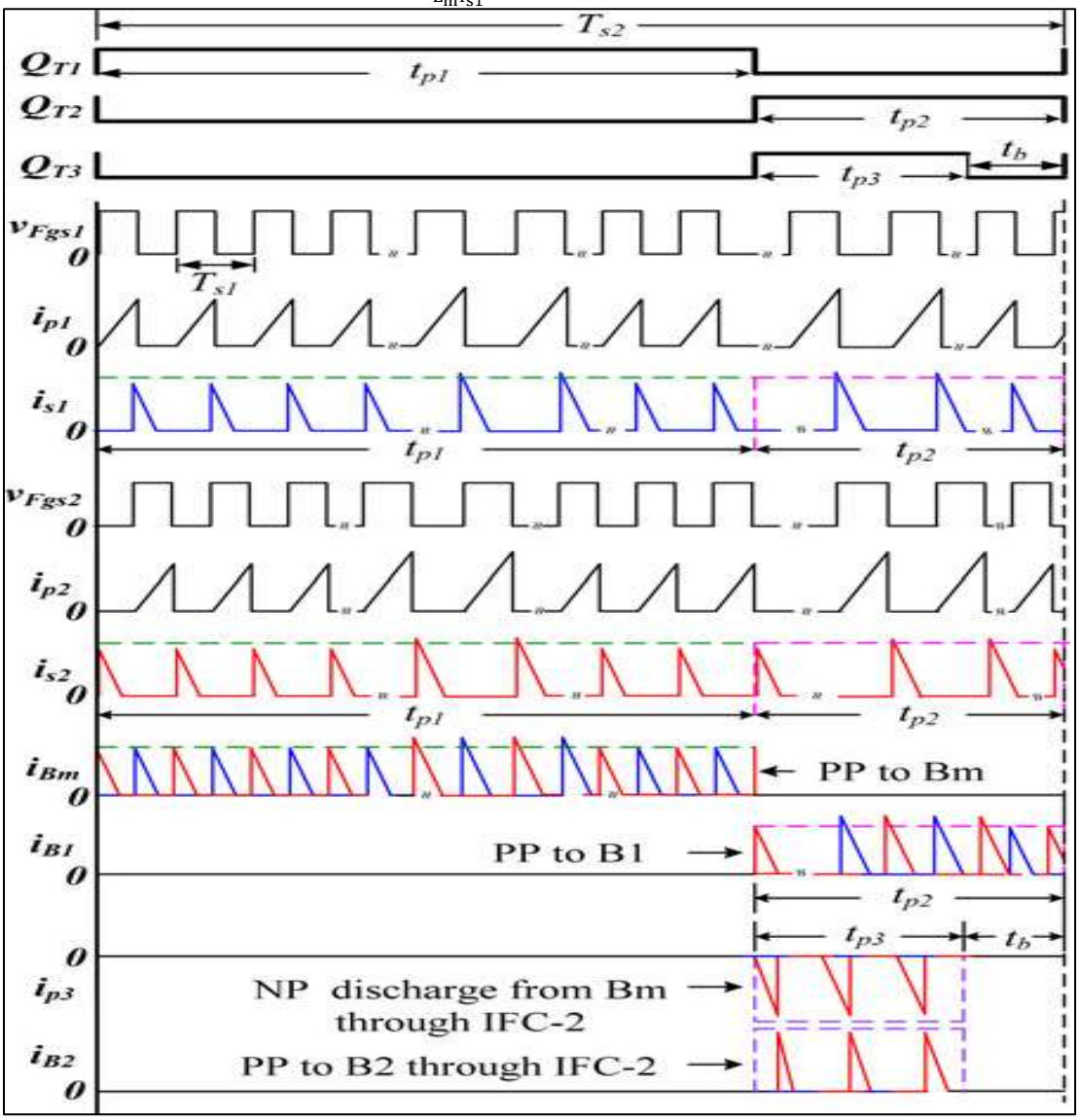

Fig. 4: Predicted charging current statuses with reference to the three power switches, QT 1, QT 2, and QT 3 in PV-BCS; including interleaved currents from PV module, ip 1 and ip 2 ; interleaved tiny pulse trains at secondary side, is1 and is2 ; tiny pulse train of PP iBm to Bm via QT 1 , and tiny pulse train of PP iB 1 to B1 via QT 2 ; intense discharging current of NP ip 3 from Bm to charge B2 with iB 2.

From (5), the control-to-output transfer function between IFC-1 and PV module can be represented by

$$\frac{I_s}{f_{s1}^{-1}} = \frac{\eta(V_{pv}d)^2}{L_m V_B} \qquad (7)$$

The circuit model of control-to-output relation between PV module and the battery can be displayed in Fig. 5(c), in which the output current I_s is inversely proportional to the control frequency f_{s1}. The simulation and experiment (from the design example) to the control-to-output model of Fig. 5(c) are shown in Fig. 6, in which all responses measured are under various solar insolation. Although the PV module is inherently capacitive, because of the diffusion and transition capacitances at high frequency, its conjugate impedance just matches the inductive impedance of the IFC-1. As a result, for attaining maximum I_s with the maximum power transfer, yield

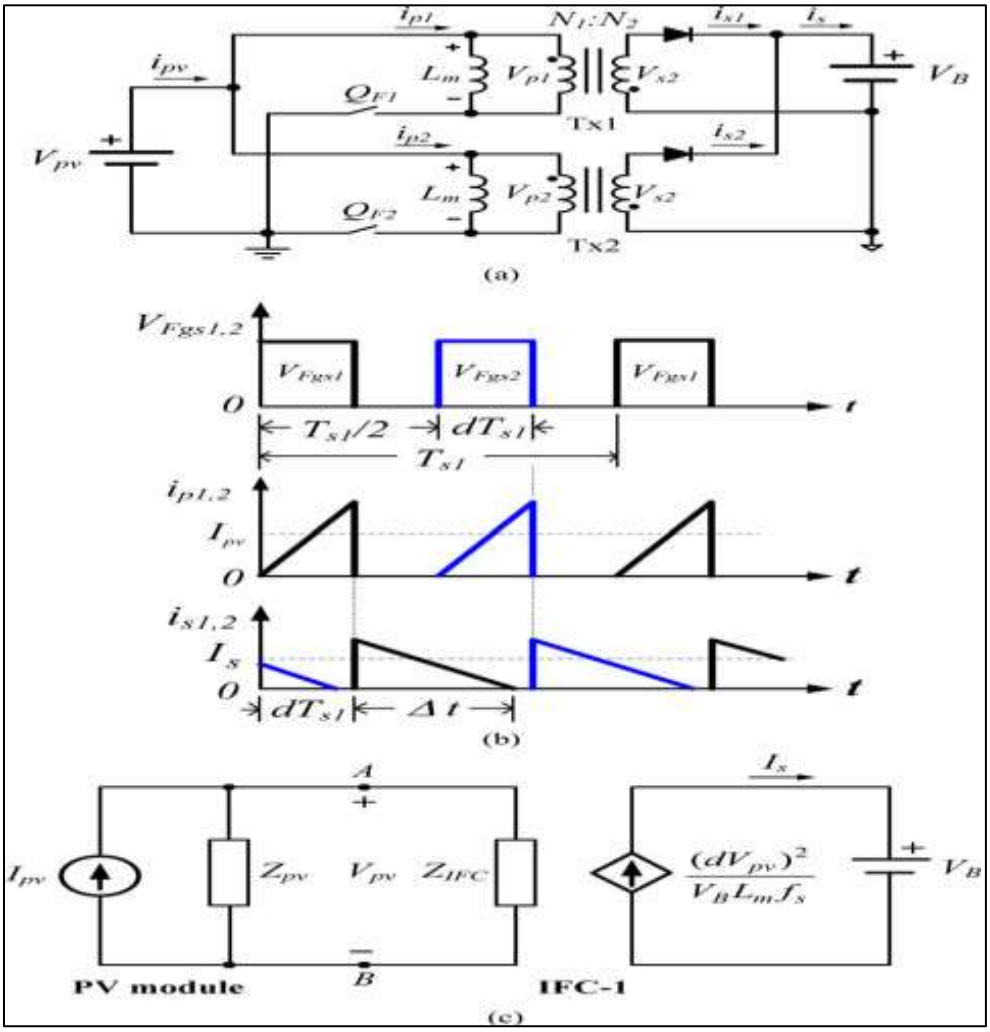

Fig. 5: (a) Simplified circuit of the PV IFC-1 loaded with a battery VB and (b) Predicted interleaved waveforms, black for QF 1 and blue for QF 2, and (c) Control-to-output Model (from PV module to battery) under maximum power transfer

$$Z_{IFC} = Z_{PV} \quad (8)$$

Where,

$$Z_{IFC} = j2\pi f_{s1} L_m \quad (9)$$

And,

$$Z_{PV} = \frac{1}{j2\pi f_{s2} C_{pv}} \quad (10)$$

Since both PV module and the IFC-1 are frequency dependent, an INC MPPT using frequency control for example is feasible for guiding the IFC-1 in energy pump. If the internal resistances between the PV module and the IFC-1 are ignored as mentioned for the analysis the $L_m C_{pv}$ relative to the switching frequency f_{s1} at maximum power transfer can then be represented by

$$L_m C_{PV} = \left(\frac{1}{2\pi f_{s1}}\right)^2 \quad (11)$$

A. Estimation of Pulse Charging Current

From Figs. 2(b) and 4, since the power switches QT1 and QT2 are complementary to the charging period Ts2, we can have

$T_{s2} = t_{p1} + t_{p2}$

$= t_{p1} + t_{p3} + t_b$

$$= (m1+m2)\, T_{s1} \quad (12)$$

where tp1 = m1Ts1 is the PP width equal to the PBP period, tp2 = m2Ts1 the non-PBP period, tp3 = m3Ts1 the NP width of, and t_b = (m2–m3s) Ts1 the pulse break time; m1, m2, and m3 are integer and the number of tiny pulses. The two average currents I_{s1} and I_{s2} from IFC-1 before synthesis can be given by, from (5)

$$I_{s1} = I_{s2} = \frac{\eta (V_{pv} d)^2}{2 V_B L_m f_{s1}} \quad (13)$$

The high-frequency tiny pulse train current i_{Bm} flows into the main Bm when $Q_{T\,1}$ turns ON in the PBP period $t_{p1} = m_1T_{s1}$. The average I_{Bm} in the low-frequency charging period, T_{s2}, as displayed in Fig. 4, can be represented by

$$I_{Bm} = \frac{m1}{m1+m2} \cdot \frac{\eta(V_{pv}d)^2}{V_{Bm}L_m f_{s1}} \qquad (14)$$

When $Q_{T\,2}$, the complementary of $Q_{T\,1}$, turns ON in the non- PBP period $t_{p2} = m_2T_{s1}$, the average current I_{B1} flowing into the battery B1 is obtained as

$$I_{B1} = \frac{m1}{m1+m2} \cdot \frac{\eta(V_{pv}d)^2}{V_{B1}L_m f_{s1}} \qquad (15)$$

Then, the average intense discharging current $I_{Bm,d}$ drawn from the Bm through IFC-2 in the NP period $t_{p3} = m_3T_{s1}$, which is equivalent to the average charging current to the B2, is given by

$$I_{Bm,d} = \frac{V_{Bm}d^2}{L_m f_{s1}} \qquad (16)$$

Since all parameters of both IFC-1 and IFC-2 are presumed to be identical, the dynamic states of IFC-2 are the same as those in Fig. 5(b), from (16), the average discharging current I_{p3} is then given by

$$I_{p3} = \frac{m3}{m1+m2} \cdot \frac{V_{Bm}d^2}{L_m f_{s1}} \qquad (17)$$

Accordingly, the average current I_{B2} that charges the B2 through IFC-2 in the charging period T_{s2}, can then be given by

$$I_{B2} = \frac{m3}{m1+m2} \cdot \frac{\eta(V_{Bm}d)^2}{V_{B2}L_m f_{s1}} \qquad (18)$$

where the efficiency η of IFC-2 is involved.

IV. INCREMENTAL-CONDUCTANCE MPPT (USING VFCD)

An INC-MPPT working in the PV-BCS is due to its attractive tracking suited to the situation that is subject to random solar insolation. Subsequently several approaches have been presented to encourage the INC-MPPT applied in PV relative systems, because its conductance-increment method can bring about accurate tracking ability to against random solar insolation. In this paper, the INC MPPT using VFCD control is presented to guide the IFC-1 to match the PV module at maximum power transfer and pumping energy at optimum MPPT. A typical PV module using Kyocera KC130T is used as design example, in which I_{pv}–V_{pv} and P_{pv}–V_{pv} characteristics are shown in the first quadrant of Fig. 6 with three kinds of solar insolation considered. If the shunt resistance R_{sh} in the model of a PV cell is neglected, the I_{pv}–V_{pv} relationship can be described by

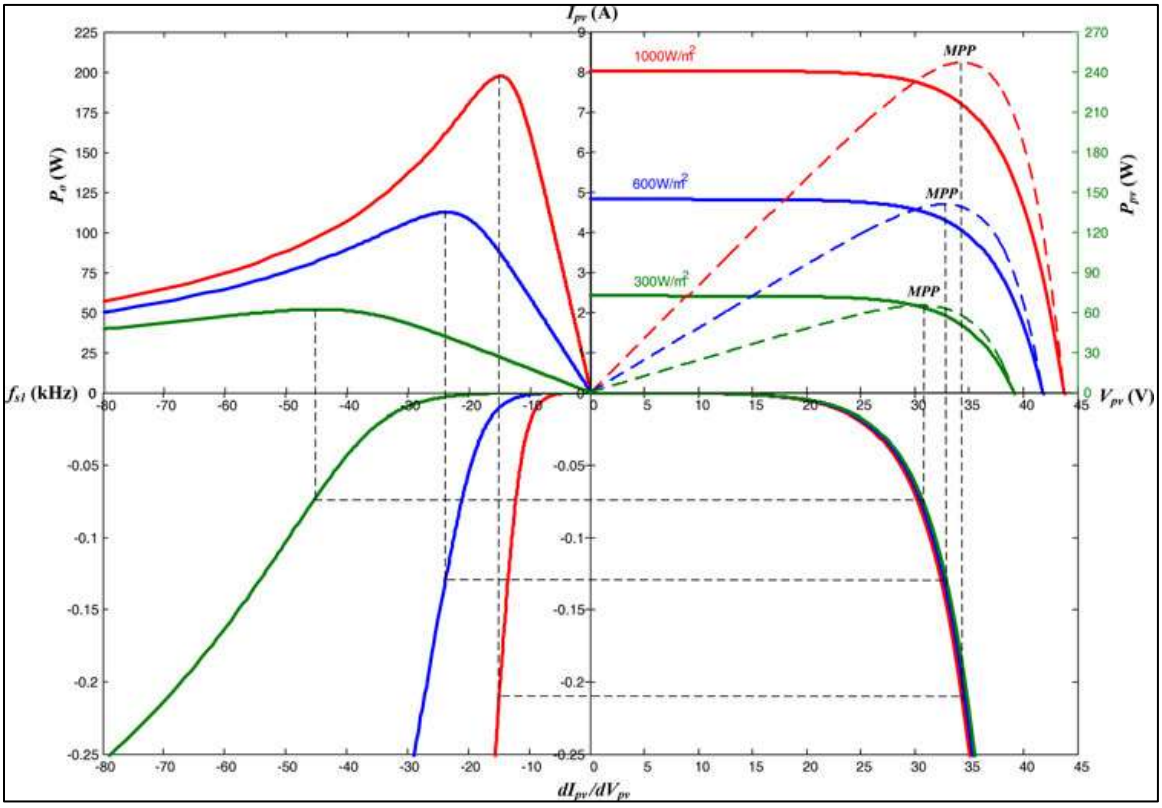

Fig. 6: Tracking chart of INC MPPT using VFCD control with duty d = 0.25, including enlarged dIpv /dVpv , Ipv, Ppv , and Po with respect to Vpv and fs1, respectively.

$$I_{pv} = I_{ph} - I_{pvo}\left\{\exp\left[\frac{q}{AkT}\left(V_{pv} + I_{pv}R_s\right)\right] - 1\right\} \qquad (19)$$

And

$$V_{pv} = \frac{AkT}{q}\ln\left(\frac{I_{ph} - I_{pv} + I_{pvo}}{I_{pvo}}\right) - I_{pv}R_s \qquad (20)$$

where I_{ph} denotes light-generated current; I_{pvo} is dark saturation current; I_{pv} is PV electric current; V_{pv} is PV voltage; R_s is series resistance; A is the non-ideality factor; k is Boltzmann's constant; T is temperature, and q is the electronic charge. The output power from the PV cell can then be given by

$P_{pv} = V_{pv}I_{pv}$

$$= I_{pv}\left\{\frac{AkT}{q}\ln\left(\frac{I_{ph} - I_{pv} + I_{pvo}}{I_{pvo}}\right) - I_{pv}R_s\right\} \qquad (21)$$

A tracking chart of the INC MPPT depicted in Fig. 6 for the aid of algorithm includes the PV converter output power P_o derived in (6), the derived dI_{pv}/dV_{pv}, I_{pv}–V_{pv}, and P_{pv}–V_{pv} with reference to the V_{pv} and control frequency. All curves in Fig. 6 are subject to three kinds of solar insolation, in which the PV characteristic is displayed in the first quadrant; the output power P_o to control frequency f_{s1} in the second quadrant; the enlarged conductance dI_{pv}/dV_{pv} versus V_{pv} in the fourth quadrant; a linkage transfer curve derived in (3) between the three quadrants in the third quadrant.

V. DESIGN CONSIDERATIONS

A. Charge Management

As stated in Fig. 2(b), the pair of complementary power switches, Q_{T1} and Q_{T2}, is to manage the chargings of Bm and B1 for relishing the remaining PV energy in the non-PBP period. The pass switch Q_{T3} is to link IFC-2 between Bm and B2 for intensely discharging the Bm and in turn charging the B2, achieving energy recovery. To date, there is indeed no way to definitely regulate how wide the pulse width is suitable for pulse charging. Then reported that the effect of pulse charging efficiency seems unchanged for a variety of duty changes. In other words, the desired pulse width can be empirically inferred from the effect of averaged charge capacity, related to the battery characteristics, such as temperature rise, permissible peak charging current, and maximum charging current. In this proposal, the smart CM dominants the burp charge for Bm in the BP period T_{s2} is specified as follows: 80% of T_{s2} for the PP charge via Q_{T1}, 10% of T_{s2} for the NP in intense discharge via Q_{T3}, and 10% of T_{s2} for the pulse break time. In other words, B1 will be charged the remaining PP energy from PV module via Q_{T2} in the non-PBP period, which is 20% of T_{s2}; B2 will receive the discharge amount from Bm via Q_{T3} in NP period, 10% of T_{s2}. Three gassing voltage detections are embedded in CM for online monitoring the battery statuses with a gassing reference of 13.8 V.

B. Interleaved IFC

In this proposal, a flyback converter selected as PV converter for example is because of its flexibility and simple topology for convenience in describing the proposed conceptual theme, especially easy to describing the impedance match between the PV module, IFC-1, and battery. In reality, the MPPT with frequency control is suited for the IFC-1 that makes impedance match between PV module and battery. The smart CM configures the IFC-1 with VFCD control guided by INC MPPT, but the IFC-2 responsible for energy recovery from Bm can be either single or interleaved topology with constant-frequency control. In addition, the two IFCs are both designed to operate in DCM so as to avoid overlap between adjacent tiny pulses. Indeed, the break time between adjacent tiny pulses will also benefit delaying the sulphating crystallization on the pores of the positive and negative electrodes of LAB.

C. Algorithm of INC MPPT

The algorithm program of INC MPPT is executed by Microchip dsPIC33FJ06GS202 according to the tracking chart in Fig. 7 and the flowchart in Fig. 8. A further contribution to the tracking algorithm is using the tracking judgment $\Delta I_{pv}V_{pv} + \Delta V_{pv} I_{pv} = ?$ rather than the usual comparison $\Delta I_{pv}/\Delta V_{pv} + I_{pv}/V_{pv} = ?$ in case the possible uncertainty $\Delta I/\Delta V$ happens when ΔV_{pv} approaches zero, ensuring the tracking of INC MPPT without interrupt. Moreover, an execution direction Dn introduced is to easily guide the frequency of IFC-1 that draws energy from the PV module to tracking optimum by following two rules: 1) execution direction Dn = 0 means reducing PV current through increasing the frequency of IFC-1; 2) execution direction Dn = 1 means increasing PV current through reducing the frequency of IFC-1.

VI. DESIGN AND EXPERIMENT

Referring to the circuit structure in Fig. 2(a), an experimental setup for a laboratory-demonstrated PV-BCS is equipped with a 250W PV module (two-in-one module) and three LABs, NF50B (2)4LS, KAWASAKI, with 45AH each. The PV-BCS provides a high-frequency tiny pulse train from PV module through the IFC-1 with maximum peak current 28 A at 1 kW/m2 for the PBP charge to Bm and PP charge to B1. In the non-PBP period, the intense discharge to the main Bm executes with a peak current of 32 A through IFC-2. In the mentioned case, both IFC-1 and IFC-2 are operated at 14.63 kHz with a duty ratio of 0.25, but the frequency of IFC-2 will keep unchanged because of independent source from Bm. For managing the charge to the three batteries,

the pair of complementary power switches, QT 1 and QT 2, and pass switch QT 3 are to operate at the suggested 550 Hz. The PBP width, tp1, for charging Bm is designed to be 80% of the BP period Ts2 (=1/fs2) and the PP width, tp2 , for B1 is 20% of Ts2.

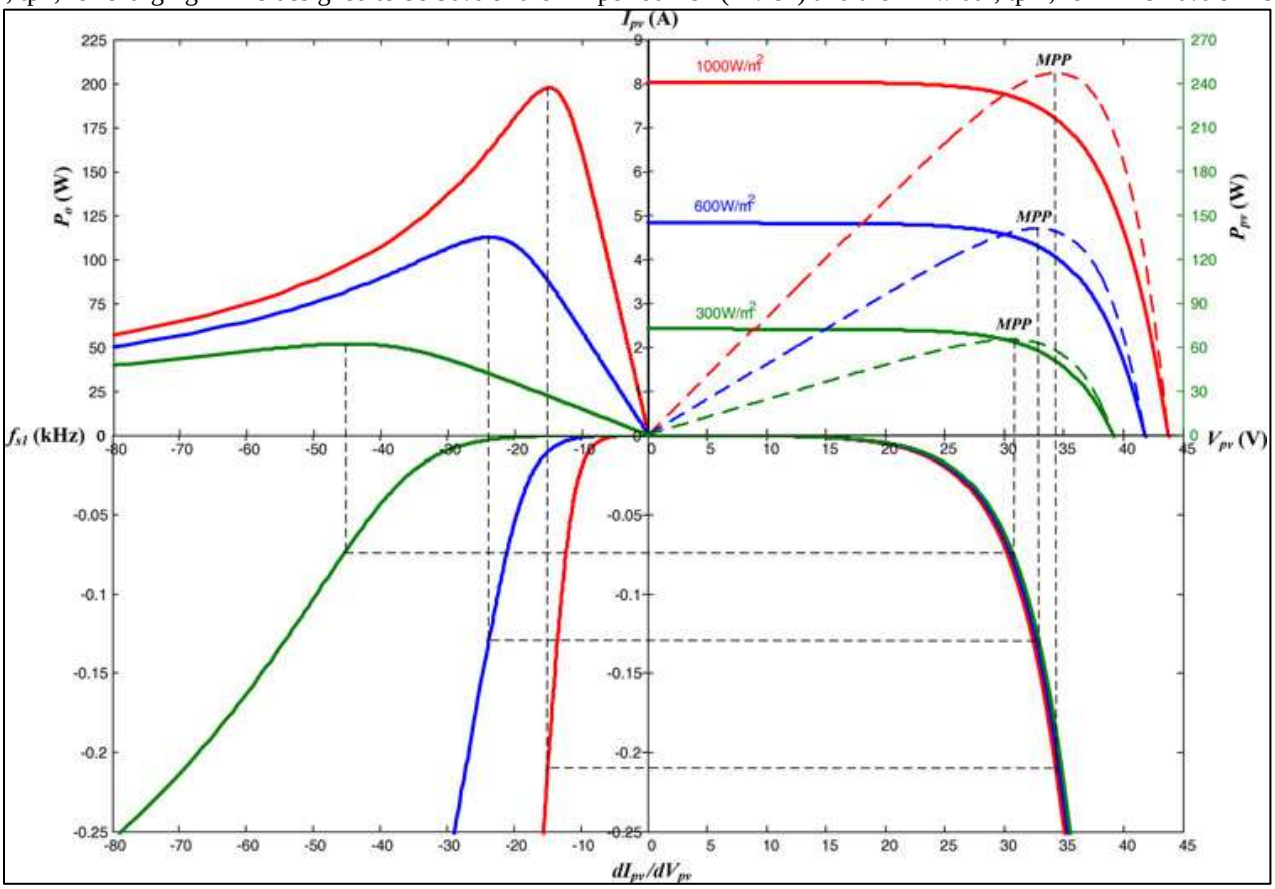

Fig. 7: Tracking chart of INC MPPT using VFCD control with duty d = 0.25, including enlarged dIpv /dVpv , Ipv, Ppv , and Po with respect to Vpv and fs1 , respectively.

The NP width, the intense discharge time, is 10% of Ts2. The BP break time tb for relaxing the Bm is 10% of Ts2. Each Kyocera KC130 T for the PV module has an open voltage 21.9 V and a short circuit current 8.2 A at 1 kW/m2. As shown in the first quadrant of Fig. 7, Ipv–Vpv and Ppv–Vpv characteristics of the PV module are measured under various solar insolation at T = 25◦C (55◦C). Their data at maximum power point (MPP) are obtained as follows: Vpv = 30.4 V (29.5 V) and Ipv = 2.14 A (2.12 A) at 300 W/m2, where fs1 = 44.43 kHz (43.44 kHz); Vpv = 32.7 V (32.0 V); at Ipv = 4.30 A (4.28 A) at 600 W/m2, where fs1 = 23.75 kHz (23.35 kHz); Vpv = 34.3 V (33.7 V), and at Ipv = 5.95 A (5.9 A) at 1 kW/m2, where fs1 = 14.63 kHz (14.66 kHz). For operating the IFCs in DCM, the magnetizing inductance of the interleaved transformer is to be Lm = 20 μH at 1 kW/m2. The algorithm of the INC MPPT is executed using Microchip dsPIC33FJ06GS202, according to the tracking algorithm in Fig. 8. Three kinds of solar insolation, 300 W/m2, 600 W/m2, and 1 kW/m2, for verifying the tracking and charging behaviours of the PV-BCS are conducted with an emulated solar power source by Chroma ATE-62150 H-600 S. The control-to-output characteristics IFC-1 are simulated (solid-line) and experimented (black dotted-line) as displayed in Fig. 6, in which the Po versus frequency fs1 characteristic is also involved in Fig. 7 to enhance the tracking ability in program algorithm. The gassing voltage reference, embedded in CM controller, is set to be 13.8 V in this design, which corresponds to 100% SOC for a 45-A sealed-maintenance-free battery of NF50B (2) 4LS KAWASAKI. An open voltage of 13 V, equivalent to 85% SOC, before gassing is used to be the measure reference for experiment.

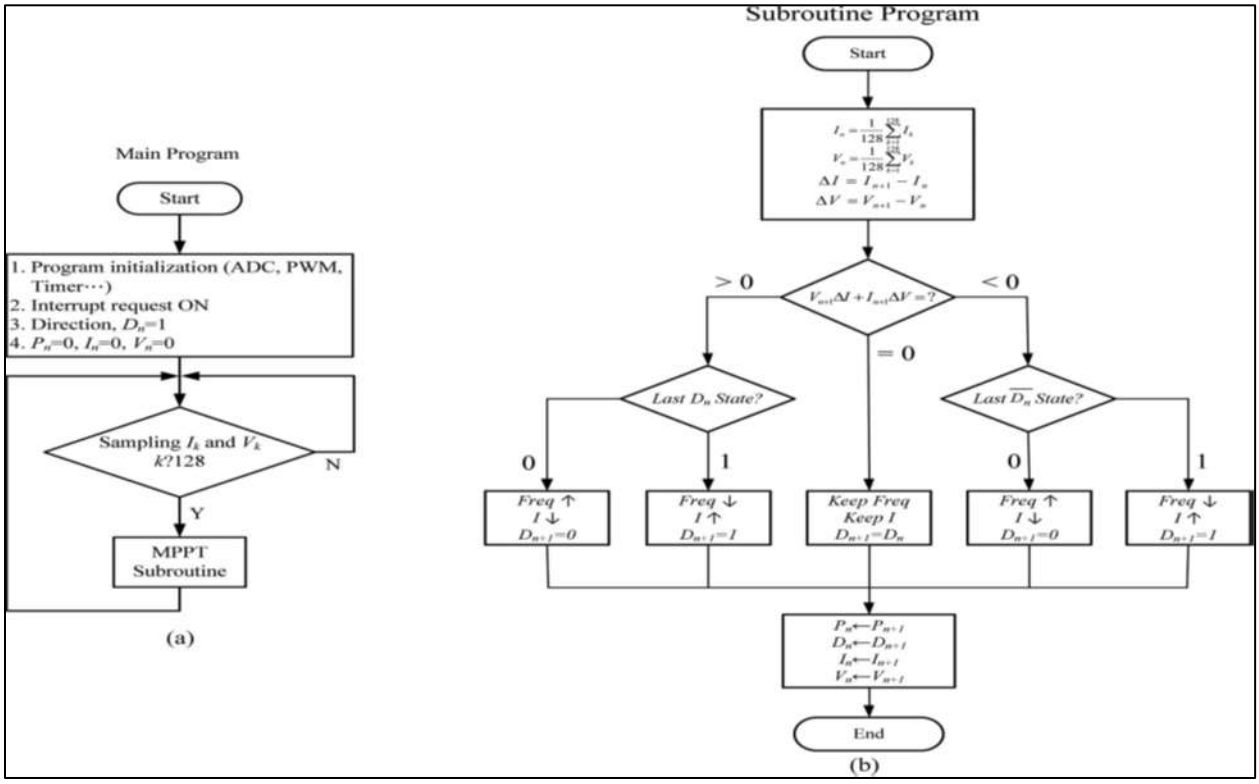

Fig. 8: Flow chart of INC MPPT algorithm: (a) Main program and (b) Subroutine program.

The control-to-output characteristics IFC-1 are simulated (solid-line) and investigated (black dotted-line) as presented in Fig. 6, in which the P_o versus frequency f_{s1} characteristic is also involved in Fig. 7 to enhance the tracking ability in program algorithm. The gassing voltage reference, embedded in CM controller, is set to be 13.8 V in this design, which resembles to 100% SOC for a 45A sealed-maintenance-free battery of NF50B (2) 4LS KAWASAKI. An open voltage of 13 V, equivalent to 85% SOC, before gassing is used to be the measure reference for experiment.

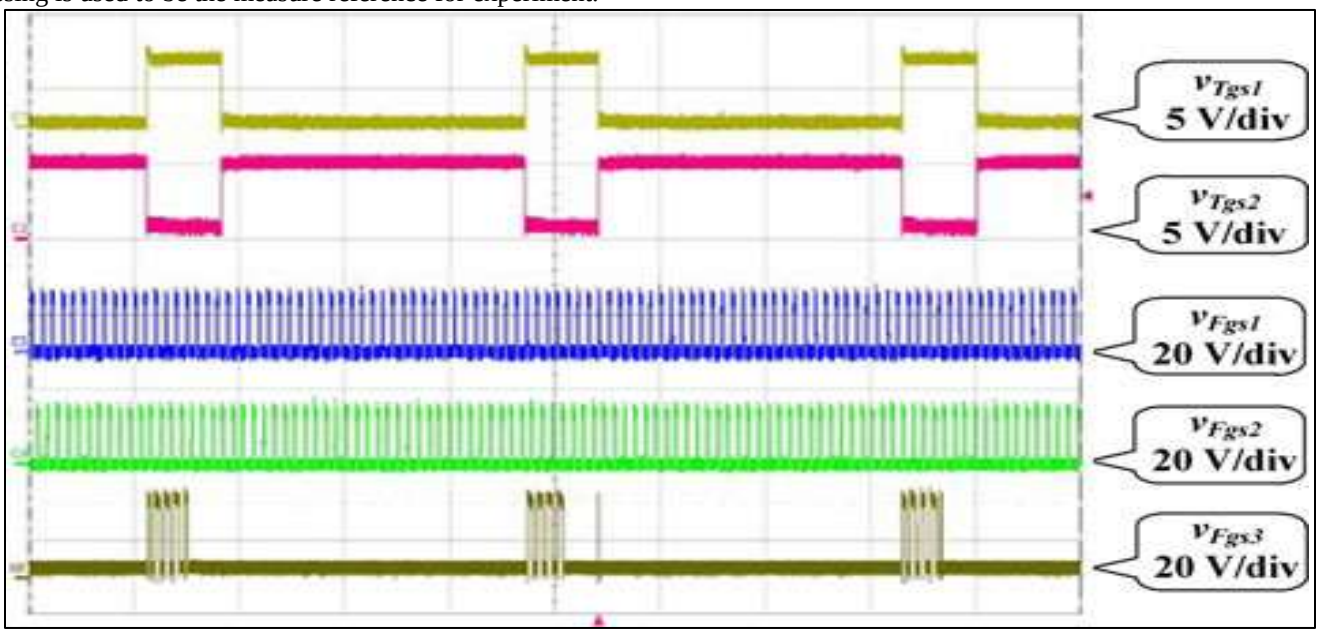

Fig. 9: Measured drive waveforms, including the complementary power switch pair, QT 1 and QT 2, with low-frequency of 550 Hz; and the three gate signals for QF 1, QF 2 , and QF 3 of IFCs in free state at high-frequency of 20 kHz before MPPT tracking, where Hor: 500 μs/div.

Fig. 9 displays the gate waveforms of QT 1 and QT 2 that operate at a low frequency of 550 Hz, and those of QF 1, QF 2 and QF 3 of the IFCs' at a high frequency of 20 kHz, in which the IFCs' frequencies are for free state before MPPT tracking. Moreover, the pulse amplitudes of the charging current iBm and iB1 are unchanged before and after the transition, but they have only a small variation at the switching instant; this means that the MPPT is always activating to continue tracking without affected by the gate

switch. In addition, the wire connection between IFCs and batteries should be as short as possible in practice so as to prevent from EMI interference.

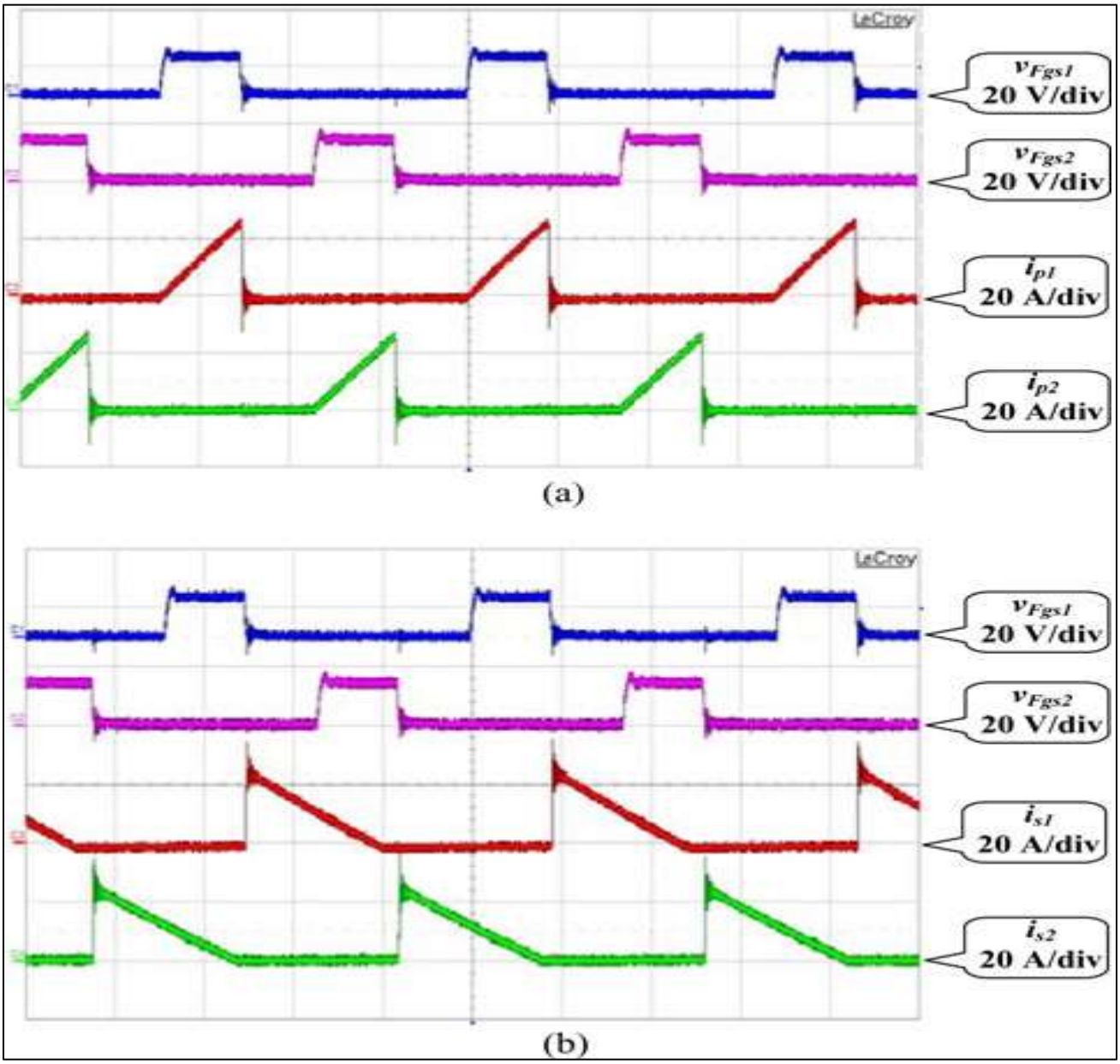

Fig. 10: Measured interleaved high-frequency tiny pulses from IFC-1 at 1 kW/m2 and fs1 = 14.63 kHz: (a) Primary currents (ip 1 , ip 2) and (b) Secondary currents (is1 , is 2), all with peak current of 26 A, Hor: 20 μs/div, (turns ratio of the transformer N1 /N2 = 1).

Fig. 10(a) shows the interleaved high-frequency tiny pulse currents (ip1, ip2) drawn from the PV module at the primary of the IFC-1. Fig. 10(b) shows that the interleaved currents (is1, is 2) generated in secondary side are synthesized at node M as the pulse train is. The is split into a PP for Bm and PP for B1 through the complementary switches, in which all waveforms are measured at MPP at 1 kW/m2.

VII. CONCLUSION

In this paper, the PV-BCS performs that the pulse charge can be realized by directly using renewable energy supply without dc bus through a dc/dc converter for buffer regulation. The idea of concurrently charging three batteries by utilizing direct renewable source creates a new theme, which makes it come true to achieve the energy treasuring and recovery concept. Except for a large-scale energy management to the battery charge, even in a remote area, the PV-BCS can also be a hybrid charger for renewable energy application if additional renewable energy is mixed with the PV energy. Especially different from a general hybrid charging mode, which always requires a dc bus as an energy buffer, the proposed PV-BCS emphasizes directly using PV energy supply without dc bus. In addition, despite the advantage of low-frequency pulse break aided for prolonging the battery life, the tiny brief break between the adjacent high-frequency pulses also benefits the dissolve of sulphating crystallization. The experiment also

evidences it feasible that the charging behaviours of PV-BCS under INCMPPT guidance can actually perform pulse charge using direct PV energy, which contributes energy saving and cherishing, especially for the way to energy storage utilizing renewable energy.

REFERENCES

[1] J. Szymborski and M. L. Eggers, "Development of a totally maintenance free lead-acid battery for telecommunications standby power," in Proc. IEEE Int. Telecommun. Energy Conf., Oct. 1982, pp. 410–415.
[2] Z. M. Salameh,M. A. Casacca, andW. A. Lynch, "A mathematical model for lead-acid batteries," IEEE Trans. Energy Convers., vol. 7, no. 1, pp. 93– 98, Mar. 1992.
[3] M. Cug, J. Sabatier, S. Laruelle, S. Grugeon, B. Sahut, A. Oustaloup, and J. M. Tarascon, "On lead-acid-battery resistance and cranking-capability estimation," IEEE Trans. Ind. Electron., vol. 57, no. 3, pp. 909–917, Mar. 2010.
[4] Y. H. Sun, H. L. Jou, and J. C. Wu, "Aging estimation method for lead acid battery," IEEE Trans. Energy Convers., vol. 26, no. 1, pp. 264–271, Mar. 2011.
[5] R. C. Harwood, V. S. Manoranjan, and D. B. Edwards, "Lead-acid battery model under discharge with a fast splitting method," IEEE Trans. Energy Convers., vol. 26, no. 4, pp. 1109–1117, Dec. 2011.
[6] M. Shahriari and M. Farrokhi, "Online state-of-health estimation of VRLA batteries using state of charge," IEEE Trans. Ind. Electron., vol. 60, no. 1, pp. 191–202, Jan. 2013.
[7] L. T. Lam,H.Ozgun, O. V. Lim, J. A. Hamilton, L. H.Vu,D. G.Vella, and D. A. J. Rand, "Pulsed-current charging of lead/acid batteries—A possible means for overcoming premature capacity loss?" J. Power Sources, vol. 53, pp. 215–228, 1995.
[8] J. J. A. Wilkinson and G. A. Covic, "A new pulse charging methodology for lead acid batteries," IPENZ Trans., vol. 25, no. 1/EMCh, pp. 1–16, 1998.
[9] S. Minami, Y. Onishi, S. J. Hou, and A. Kozawa, "A new intense pulse charging method for the prolongation of life in lead-acid batteries," J. Asian Electric Vehicles, vol. 2, no. 1, pp. 541–544, 2004.
[10] S. J. Hou, Y. Onishi, S. Minami, H. Ikeda, M. Sugawara, and A. Kozawa, "Charging and discharging method of lead acid batteries based on internal voltage control," J. Asian Electric Vehicle, vol. 3, no. 1, pp. 733–737, 2005.
[11] H. Ikeda, S. Minami, S. J. Hou, Y. Onishi, and A. Kozawa, "Nobel high current pulse charging method for prolongation of lead-acid batteries," J. Asian Electric Vehicle, vol. 3, no. 1, pp. 681–687, 2005.
[12] M. Bhatt,W. G. Hurley, andW. H.W¨olfle, "A new approach to intermittent charging of valve-regulated lead–acid batteries in standby applications," IEEE Trans. Ind. Electron., vol. 52, no. 5, pp. 1337–1342, Oct. 2005.
[13] S. J. Hou, H. Ikeda, Y. Takai, S. Minami, A. Kozawa, M. Sugawara, and T. Nishina, "Experimental study on the optimum density of ITE additives for a lead-acid battery's life prolongation," J. Asian Electric Vehicle, vol. 4, no. 2, pp. 939–946, 2006.
[14] L.R. Chen, "Design of duty-varied voltage pulse charger for improving lion battery-charging response," IEEE Trans. Ind. Electron., vol. 56, no. 2, pp. 480–487, Feb. 2009.
[15] R. Wang, F. Wang, D. Boroyevich, R. Burgos, R. Lai, P. Ning, and K. Rajashekara, "A high power density single-phase PWM rectifier with active ripple energy storage," IEEE Trans. Power Electron., vol. 26, no. 5, pp. 1430–1443, May 2011.
[16] L. R. Chen, S. L. Wu, D. T. Shieh, and T. R. Chen, "Sinusoidal-ripple current charging strategy and optimal charging frequency study for Li-Ion batteries," IEEE Trans. Ind. Electron., vol. 60, no. 1, pp. 88–97, Jan. 2013.
[17] S. J. Huang, B. G. Huang, and F. S. Pai, "Fast charge strategy based on the characterization and evaluation of LiFePO4 batteries," IEEE Trans. Power Electron., vol. 28, no. 4, p. 1555-1562, Apr. 2013.
[18] W. X. Zeng, J. Ma, andY. Zhai, "Rapid charge system for lead-acid battery of solar energy street light based on single-chip microcomputer," in Proc. Int. Conf. Comput. Sci. Inf. Tech., 2008, pp. 337–341.
[19] B. Y. Chen and Y. S. Lai, "New digital-controlled technique for battery charger with constant current and voltage control without current feedback," IEEE Trans. Ind. Electron., vol. 59, no. 3, pp. 1545–1553, Mar. 2012.
[20] J. H. Lee, H. S. Bae, and B. H. Cho, "Resistive control for a photovoltaic battery charging system using a microcontroller," IEEE Trans. Ind. Electron., vol. 55, no. 7, pp. 2767–2775, Jul. 2008.
[21] M. Ashwin and V. S. Vignesh, "Modified photovoltaic battery charging system using microcontroller based on resistive control," in Proc. IEEE Annu. India Conf., 2011, pp. 1–6.
[22] K. Y. Lo, Y. M. Chen, and Y. R. Chang, "MPPT battery charger for standalone wind power system," IEEE Trans. Power Electron., vol. 26, no. 6, pp. 1631–1638, Jun. 2011.
[23] H. Shen, X. Wang, J. Wang, Y. Xie, and W. Wang, "Vision based battery exchange robots for electric vehicle," in Proc. Int. Conf. Mechatronics Autom., Aug. 2012, pp. 2472–2476.
[24] G. Byeon, T. Yoon, S. Oh, and G. Jang, "Energy management strategy of the DC distribution system in buildings using the EV service model," IEEE Trans. Power Electron., vol. 28, no. 4, pp. 1544–1554, Apr. 2013.
[25] Wasynczuk, "Dynamic behavior of a class of photovoltaic power system," IEEE Trans. Power Apparatus Syst., vol. PAS-102, no. 9, pp. 3301–3307, Sep. 1983.
[26] K. H. Hussein, I. Muta, T. Hoshino, and M. Osakada, "Maximum photovoltaic power tracking: an algorithm for rapidly changing atmospheric," IEE Proc. Gener. Transmiss. Distrib., vol. 142, no. 1, pp. 59–64, Jan. 1995. 1790 IEEE TRANSACTIONS ON POWER ELECTRONICS, VOL. 29, NO. 4, APRIL 2014
[27] D. Chenvidhya, K. Kirtikara, and C. Jivacate, "PV module dynamic impedance and its voltage and frequency dependencies," Solar Energy Mater. Solar Cells, vol. 86, no. 2, pp. 243–251, 2005.
[28] T. Esram and P. L. Chapman, "Comparison of photovoltaic module maximum power point tracking techniques," IEEE Trans. Energy Convers., vol. 22, no. 2, pp. 439–449, Jun. 2007.
[29] G. C. Hsieh,H. L. Chen,Y. H. Chen, C. M. Tsai, and S. S. Shyu, "Variable frequency controlled incremental conductance derived MPPT photovoltaic stand-alone DC bus system," in Proc. IEEE Appl. Power Electron. Conf. Expo, Austin, TX, USA, Feb. 2008, pp. 1849–1854.
[30] F. Liu, S. Duan, F. Liu, B. Liu, and Y. Kang, "A variable step size INC MPPT method for PV systems," IEEE Trans. Ind. Electron., vol. 55, no. 7, pp. 2622–2628, Jul. 2008.
[31] G. C. Hsieh, C. Y. Tsai, and Chen, "Interleaved smart burp PV charger for lead acid batteries with incremental conductance MPPT," in Proc. IEEE Energy Convers. Congr. Expo., Arizona, Sep. 2011, pp. 3248–3255.
[32] J. Zhao, H Zhao, and F. Dai, "A novel ZVS PWM interleaved flyback converter," in Proc. IEEE 2nd Conf. Ind. Electron. Appl., 2007, pp. 337– 341.